Coexistence of spherical states with deformed and superdeformed bands in doubly magic ^{40}Ca; A shell model challenge.

E. Caurier [*], J. Menéndez [+], F. Nowacki [*] and A. Poves [+]

(*) IReS, Bât27, IN2P3-CNRS/Université Louis Pasteur BP 28, F-67037 Strasbourg Cedex 2, France

(+) Departamento de Fisica Teórica, C-XI. Universidad Autónoma de Madrid, E-28049, Madrid, Spain

(Dated: February 9, 2008)

Large scale shell model calculations, with dimensions reaching 10^9, are carried out to describe the recently observed deformed (ND) and superdeformed (SD) bands based on the first and second excited 0^+ states of ^{40}Ca at 3.35 MeV and 5.21 MeV respectively. A valence space comprising two major oscillator shells, sd and pf, can accommodate most of the relevant degrees of freedom of this problem. The ND band is dominated by configurations with four particles promoted to the pf-shell (4p-4h in short). The SD band by 8p-8h configurations. The ground state of ^{40}Ca is strongly correlated, but the closed shell still amounts to 65%. The energies of the bands are very well reproduced by the calculations. The out-band transitions connecting the SD band with other states are very small and depend on the details of the mixing among the different np-nh configurations, in spite of that, the calculation describes them reasonably. For the in-band transition probabilities along the SD band, we predict a fairly constant transition quadrupole moment $Q_0(t) \sim 170$ e fm^2 up to J=10, that decreases toward the higher spins. We submit also that the J=8 states of the deformed and superdeformed band are maximally mixed.

I. INTRODUCTION

^{40}Ca is a textbook example of doubly magic nucleus, corresponding to neutrons and protons filling the three lowest harmonic oscillator shells with principal quantum numbers p=0, 1, and 2. The N=Z=20 gap is large (about 7 MeV) and therefore, in a naive independent particle description, its spectrum will consist of negative parity quasi degenerated states starting at an excitation energy commensurable with the value of the gap and positive parity states at about twice the value of the gap. Indeed, this is not the case and its first excited state is a 0^+ at 3.35 MeV, that turns out to be the head of a deformed band. Excited deformed bands in spherical nuclei provide a spectacular example of coexistence of very different structures at the same energy scale, that is a rather peculiar aspect of atomic nuclei. Other cases have been known for a long time, for instance, the four particle four holes and eight particle eight holes states in ^{16}O, starting at 6.05 MeV and 16.75 MeV of excitation energy [1, 2]. The theoretical descriptions based in multiple particle hole excitations that can accommodate deformation started with the work of Brown and Green [3], Gerace and Green [4, 5] and Zuker, Buck and McGrory [6] In ^{40}Ca, there has been since long experimental indications showing that the two low-lying sequences, 0^+, 2^+, 4^+, starting at 3.35 MeV and 5.21 MeV, may correspond to deformed or superdeformed bands (see ref. [7]). However, it is only recently that such bands, deformed and superdeformed, have been explored up to high spins, in several medium-light nuclei such as ^{56}Ni [8], ^{36}Ar [9] and of course ^{40}Ca [10], thanks to the availability of large arrays of γ detectors like Euroball and Gammasphere.

One characteristic feature of these bands is that they may belong to rather well defined shell model configurations; for instance, the deformed excited band in ^{56}Ni can be associated with the configuration $(0f_{7/2})^{12}$ $(1p_{3/2}, 0f_{5/2}, 1p_{1/2})^4$ while the super-deformed band in ^{36}Ar is based in the structure $(sd)^{16}$ $(pf)^4$. The location of the np-nh states in ^{40}Ca was studied in the Hartree-Fock approximation with blocked particles and Skyrme forces in ref. [11]. While many approaches are available for the microscopic description of these bands (Cranked Nilsson-Strutinsky [9], Hartree-Fock plus BCS with configuration mixing [12], Angular Momentum Projected Generator Coordinate Method [13], Projected Shell Model [14], Cluster models [15, 16] etc.) the interacting shell model is, when affordable, a prime choice. The mean field description of $N = Z$ nuclei, has problems related to the correct treatment of the proton-neutron pairing in its isovector and isoscalar channels, as well as the proper restoration of the symmetries broken at the mean field level to take into account the pairing (particle number) and quadrupole (angular momentum) correlations. In addition, the triaxial degrees of freedom are seldom considered. On the shell model side, the problems come from the size of the valence spaces needed to accommodate the np-nh configurations.

In a recent article [17], it was shown that large scale shell model calculations within a valence space consisting on the sd and pf shells can describe the coexistence of the spherical ground state and the superdeformed band of ^{36}Ar, both the very existence of the spherical and the superdeformed states forming a band and the configuration mixing that permits transitions connecting them. In the same spirit, in the present work we focus on the case of ^{40}Ca, which is particularly challenging since it presents two rotational bands of different kind above the spherical ground state. The first rotational band, starting at 3.35 MeV of excitation energy, is generated by an

intrinsic deformed state, whereas the other one, starting at 5.21 MeV above the ground state, stems from an intrinsic super-deformed state, i.e. bearing an axis ratio close to 2:1.

In earlier works we have surmised that the superdeformed band corresponds to a structure $(sd)^{16} \, (pf)^8$, while the normal deformed band presents a $(sd)^{20} \, (pf)^4$ structure [18, 19]. That is, the structure of the bands corresponds to the promotion of four and eight particles across the Fermi level, from the sd to the pf shell, that we call 4p-4h and 8p-8h configurations. However, this description is too crude, because the physical states contain components of different np-nh rank. The mixing should allow for transitions connecting the superdeformed and normal deformed bands as well as both bands with the spherical ground state, while remaining gentle enough not to jeopardize the very existence of the bands. This is the aim of this work; to explain the coexistence of spherical, deformed and superdeformed structures at low energy in ^{40}Ca and to understand how do their dominant configurations mix among themselves while preserving their identity.

II. SPHERICAL MEAN FIELD *vs* CORRELATIONS

The intriguing question is how comes that these many particle-hole configurations appear so low in excitation energy. Before answering it with the actual calculation, we want to advance a more qualitative discussion based in the competition between spherical mean field and quadrupole and pairing correlations.

In a very recent paper [20] Rowe *et al.* have examined this issue in ^{16}O, with a model consisting of a spherical harmonic oscillator mean field plus an Elliott's quadrupole-quadrupole interaction. In their model, the unperturbed excitation energy of an np-nh excitation between contiguous shells is $n\hbar\omega$. With the standard prescription for $\hbar\omega$ the value of the ^{40}Ca gap is largely overestimated (12 MeV instead of the experimental 7 MeV). The quadrupole correlation energy is taken as proportional to the Casimir operator of the lowest grade SU(3) irrep corresponding to the np-nh configuration, $C_{SU(3)}$, with the coupling constant for the quadrupole-quadrupole interaction equal to $\hbar\omega/2N_0$, (N_0 being the total number of oscillator quanta in the ground state of the nucleus of interest). The excitation energy of the np-nh band-head can be written as:

$$\Delta E = \hbar\omega \left((N(np-nh) - N_0) - \frac{C_{SU(3)}}{4N_0} \right) \qquad (1)$$

For the deformed band –n=4, λ=12, μ=8– ΔE=1.06$\hbar\omega$ and for the superdeformed band –n=8, λ=20, μ=12– ΔE=0.66$\hbar\omega$ (λ and μ being Elliott's labels of the irreps of SU(3)) This model is very schematic, and, as we shall discuss later, overestimates both the energy differences

between the closed shell and the np-nh configurations at the mean field level, and the correlation energies of the later. Thus, it is not surprising that it cannot reproduce the experimental numbers. But it contains the right message; that there is a class of states, related to SU(3) configurations of maximum weight, that can gain huge amounts of correlation energy provided the structure of the spherical mean field does not hamper their collective build-up. In the present case, instead of the assumed SU(3) coupling scheme in both shells, the physical situation is closer to pseudo-SU(3) [21] in the sd shell, based in the quasi-degenerate $s_{1/2}$-$d_{3/2}$ doublet and quasi-SU(3) [22] in the pf shell, originated in the Δj=2, Δl=2 pair of orbits, $f_{7/2}$-$p_{3/2}$. This means lower symmetry and therefore less correlation energy. But this reduction is more than compensated by using a better spherical mean field, that, in particular, must incorporate quadratic monopole terms. These, as we shall see, reduce notably the mean field excitation energy of the np-nh configurations [23]. Furthermore, pairing correlations need to be taken into account as well.

In addition to the estimates of the energy gains, the above SU(3)-like models make it possible to compute the intrinsic quadrupole moments associated to the different np-np deformed structures. Using the pseudo+quasi-SU(3) prescription we find Q_0=125 e fm^2 for the 4p-4h configuration and Q_0=180 e fm^2 for the 8p-8h, consistent with what one would expect for a deformed and a superdeformed band. Let's underline that what we submit is that super-deformation in this region of nuclei can be achieved readily in the space of two major oscillator shells, provided that SU(3)-like geometries of the spherical mean field are at hand. The SU(3) limit gives Q_0=148 e fm^2 and Q_0=226 e fm^2 instead. As the quadrupole correlation energy should vary as the square of the quadrupole moment, we can reckon that the pseudo+quasi-SU(3) correlation energy represents 2/3 of the SU(3) limit.

III. VALENCE SPACE AND EFFECTIVE INTERACTION

As we have explained above, an adequate valence space for the study of the coexisting bands in ^{40}Ca consists of the sd and pf major oscillator shells. Its only drawback is that the dimensions involved (10^{12}) are beyond our present computing capability. A possible way out is to close the $d_{5/2}$ orbit, that is, to work with a virtual ^{28}Si inert core. The quadrupole colectivity of the solutions will be reduced by this truncation, but we have checked in ^{36}Ar that the effect is moderate. As a bonus, this truncation reduces drastically the spurious center of mass components of our wave functions that can therefore be controlled perturbatively. Hence, our valence space will encompass the $1s_{1/2}$, $0d_{3/2}$, $0f_{7/2}$, $1p_{3/2}$, $0f_{5/2}$ and $1p_{1/2}$ orbits, leading to maximum basis sizes of O(10^9). Following the notation of ref. [24] we call this valence space

r_2pf. In an harmonic oscillator major shell of principal quantum number p, r_p represents all the orbits except the one with the largest $j = p + \frac{1}{2}$.

For this valence space we will use the effective interaction of ref.[9], named SDPF.SM and described in detail in [24]. In addition, to reduce the effects of the mixing with states with spurious centre of mass excitations, we add to the interaction the center of mass hamiltonian, $\lambda_{CM} H_{CM}$, with $\lambda_{CM} = 0.5$. The effect of this correction is small, since the blocking of the $d_{5/2}$ orbit reduces greatly the centre of mass contamination. An unwelcome effect of the blocking of the $d_{5/2}$ orbit, we have to live with, is that it does not affect equally to the different np-nh configurations. It has none on the closed shell and becomes maximal for the 12p-12h excitations. In ref.[9] the losses of correlation energy were compensated by an attractive monopole term parabolic in n. We shall do the same in the present case, but, instead of trying to infer from partial calculations the parameters of the monopole correction, we shall adjust them so as to locate the two excited 0^+ states close to their experimental values. We discuss this issue in more detail along with the presentation of the results of the fully mixed calculations.

IV. CALCULATIONS AT FIXED N$\hbar\omega$

With the effective interaction and the valence space ready, we start by making calculations at fixed n$\hbar\omega$. The aim is to verify that our expectations based in previous experiences and in algebraic models are fulfilled. And indeed they are. In fig.1 we present the results of the $8\hbar\omega$ calculation compared with the experimental superdeformed band from ref.[10] in a backbending plot. The accord is excellent, only the slight change of slope at $J = 10$ is not reproduced by the calculation. Notice that the band is very regular, showing no backbending up to $J = 24$, contrary to the situation in ^{48}Cr or ^{36}Ar. This delay in the alignment regime is surely due to the extra collectivity induced by the presence of eight particles in quasi-$SU(3)$ orbitals -four in ^{36}Ar- and four particles in pseudo-$SU(3)$ orbitals- absent in ^{48}Cr. The tiny backbending at J=20 produced by the truncated calculation of ref. [18], disappears when the unrestricted r_2pf valence space is employed.

In table I we have collected the quadrupole properties of the superdeformed band. We have computed the $B(E2)$'s and the spectroscopic quadrupole moments Q_{spec} using the conventional effective charges $\delta q_\pi = \delta q_\nu = 0.5$ and b=1.974 fm. We extract the intrinsic (transition) quadrupole moments $Q_0(t)$ from the $B(E2)$'s and the static ones $Q_0(s)$ from the spectroscopic quadrupole moments, assuming $K = 0$ and using the standard formulas relating laboratory and intrinsic frame quantities;

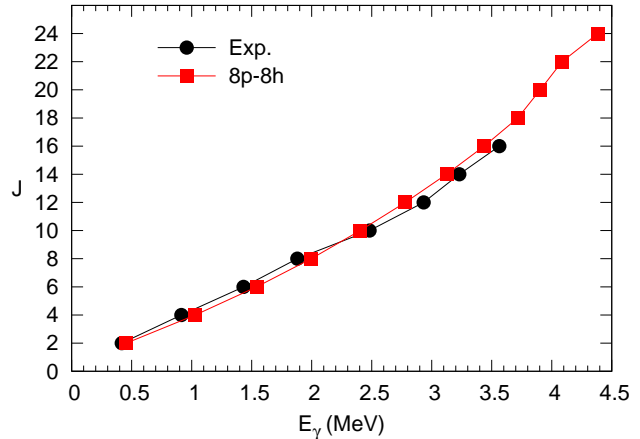$$Q_0(s) = \frac{(J+1)(2J+3)}{3K^2 - J(J+1)} Q_{spec}(J), \quad K \neq 1 \quad (2)$$

Figure 1: Superdeformed band in ^{40}Ca. E_γ's, experimental vs fixed $8\hbar\omega$ results

Table I: Quadrupole properties (in efm^2 and e^{2}fm^4) of the superdeformed band in ^{40}Ca in a fixed 8p-8h calculation.

J	$Q_{spec.}$	$B(E2)_{J \to J-2}$	Q_0(s)	Q_0(t)
2	-51.4	643	180	180
4	-64.6	905	178	178
6	-68.4	968	171	176
8	-69.6	980	165	173
10	-69.9	953	161	168
12	-70.5	896	159	162
14	-72.0	804	159	152
16	-72.5	696	159	141

$$B(E2, J \to J-2) = \frac{5\,e^2}{16\pi} |\langle JK20|J-2,K\rangle|^2 Q_0^2(t) \quad (3)$$

$$K \neq 1/2,\ 1;$$

The value of the intrinsic quadrupole moment roughly corresponds to a deformation parameter $\beta = 0.6$, which is characteristic of a superdeformed shape and agrees with the experimental value of ref.[10] (a comparison with a subsequent analysis of the same experiment [25] will be made in sections VI A and VI C). In Fig. 2 we have plotted the calculated and experimental results; they agree within the large experimental error bars. Notice that as J grows, the theoretical results lose some collectivity, whereas the experimental fit to the Doppler Shift Attenuation data is compatible with a constant transition quadrupole moment. The experimental point corresponding to the $4^+ \to 2^+$ transition comes from an earlier measure of the lifetime of the 4^+ state and its in-band branching ratio [26].

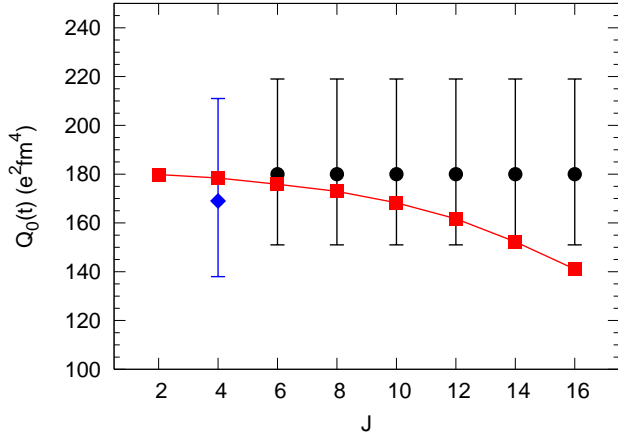The rather impressive agreement of the energetics of

Figure 2: Superdeformed band in ^{40}Ca; transition quadrupole moments $Q_0(t)$; experimental results from ref. [26] (lozenges) and from ref.[10] (circles) vs the results of the fixed 8p-8h calculation (squares).
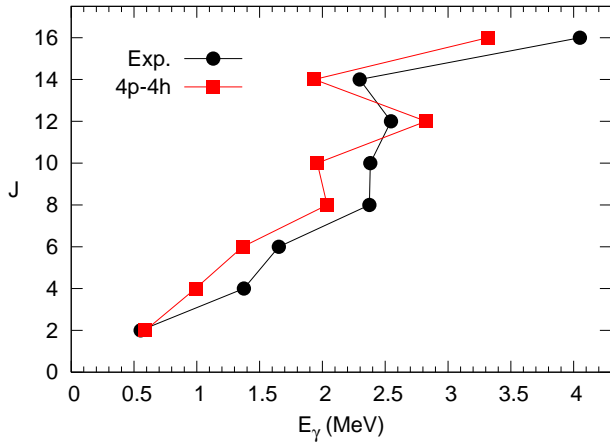

Figure 3: ND band in ^{40}Ca. E_γ's, experiment vs 4p-4h calculation.

the superdeformed band with the calculation at fixed $8\hbar\omega$ is reminiscent of what we had found in the study of ^{36}Ar and, as it was the case then, suggests that the SD band is of rather pure 8p-8h character.

We have performed as well a fixed 4p-4h calculation in order to describe the ND bands in ^{40}Ca. The most salient aspect of the calculated results is the triaxial character of the solution, with a well developped γ-band based in the second 2^+ state (2^+_γ) of the 4p-4h configuration. The results for the band based on the lowest 0^+ state of the $4\hbar\omega$ space are compared to the experimental ones from ref. [10] (band 2) in Fig. 3. The agreement is now much worse that for the SD band, although the main trends are already present in the calculation. At $J = 12$ the ex-

Table II: Comparison of the experimental transition energies (in keV) in the γ band of ^{40}Ca with the fixed $4\hbar\omega$ calculation.

Transition	E_γ(4p-4h)	E_γ(Experiment)
$3^+_\gamma \to 2^+_\gamma$	819	781
$4^+_\gamma \to 2^+_\gamma$	1244	1260
$5^+_\gamma \to 3^+_\gamma$	1187	1369
$7^+_\gamma \to 5^+_\gamma$	1501	1538
$9^+_\gamma \to 7^+_\gamma$	2346	2773
$11^+_\gamma \to 9^+_\gamma$	1518	1827
$13^+_\gamma \to 11^+_\gamma$	1943	3044

Table III: Quadrupole properties (in efm^2 and e^{2}fm^4) of the ND of ^{40}Ca in a fixed $4\hbar\omega$ calculation.

J	Q_{spec}	B(E2)$_{J \to J-2}$	$Q_0(s)$	$Q_0(t)$
2	-31.0	269	109	116
4	-41.0	364	113	113
6	-48.9	341	120	104
8	-44.0	309	104	97
10	-48.9	237	113	84
12	-38.3	86	86	50
14	-40.9	115	91	58
16	-34.8	47	76	37

perimental band upbends while the calculation produces a strong backbending.

The 2^+ band-head of the γ-band is located 2.05 MeV above the 0^+ band-head of the K=0 ND band. Experimentally the splitting is 1.90 MeV. The transition energies inside the γ-band are compared to the experimental ones, ref. [10] (band 4), in table II. The calculated values compare reasonably well with the experiment, except for the location of the 13^+ state that appears 1 MeV too low.

The quadrupole properties of the K=0 ND band are shown in table III. In this case, the corresponding deformation parameter has the value $\beta = 0.3$, a typical value for a normal deformed band. We postpone the comparison with the experimental data to the discussion of the complete calculation.

We close this section by stressing that the shell model calculations in the r_2pf valence space at fixed 8p-8h and 4p-4h configurations give a convincing description of the superdeformed band in ^{40}Ca, and are also able to describe the corresponding ND rotational spectra, which turns out to be that of a triaxial structure developing a K=0 and a K=2 (γ) band, in agreement with the experimental information. Indeed, in the physical states the configurations with different values of $n\hbar\omega$ mix, mainly through the cross shell pairing interactions, and it will be the task of the next sections to understand how this mixing proceeds and to compare the complete results with the experimental data.

V. THE ENERGIES OF THE N$\hbar\omega$ BAND-HEADS RELATIVE TO THE CLOSED SHELL

Before moving into the full r_2pf space diagonalizations, we need to explore more in depth the information gathered in the fixed N$\hbar\omega$ calculations. With the SDPF.SM interaction, the n$\hbar\omega$ bandheads lie too high in energy relative to the closed shell, as it was the case in our study of ^{36}Ar. A small part of this missing energy can be due to residual defects of the cross-shell monopole terms of the interaction, but the bulk of it is due to the blocking of the $0d_{5/2}$ orbit. We can absorb this effect via the modification of two global monopole terms:

$$\Delta(n) = \frac{1}{2}n(n-1)\delta_1 + n(12-n)\delta_2 \qquad (4)$$

where n is the number of particles in the pf-shell, and the δ's are the modifications of the global pf-shell monopole interaction and the r_2–pf monopole interaction, respectively. In our study of ^{36}Ar, an equivalent expression was used. In a first set of exploratory calculations, we realized that when the δ's were chosen so as to locate the two excited 0^+ states at about their experimental excitation energies, the percentage of closed shell in the ground state of ^{40}Ca was too low (54%), i. e. the mixing was too strong. In order to diminish the mixing we have multiplied all the cross shell off-diagonal matrix elements by a factor 0.8. Now, the values of the δ's that place the 0^+ states correctly are δ_1=–0.27 MeV, and δ_2=–0.130 MeV. With this choice the closed shell component of the ground state rises to 65%, that we take as a reasonable value. We have used another set of δ's that gives 75% of closed shell and no dramatic changes are observed in the ensemble of observables. As the 0.8 scaling implies a reduction of the pairing interactions in the space, the isovector pairing matrix elements of the pf-shell part of the SDPF.SM interaction, that were reduced by a factor 0.6 in our study of ^{36}Ar, are taken now as 0.8 times their SDPF.SM values. In summary, we have loosely fitted two global monopoles of the interaction to the location of the excited 0^+ states, keeping the core excited components in the 30% range. Actually, the difference in correlation energy between a full sd-shell calculation for the nucleus $N = Z = 20 - \frac{n}{2}$, and the calculation with the orbit $0d5/2$ blocked, accounts for two thirds of the value of $\Delta(n)$. The pairing modifications can be justified with perturbation theory arguments (see the discussion in [17]).

We have now all the ingredients needed to make quantitative the discussion of sec. II. They are plotted in Fig. 4. The squares give the lowest uncorrelated energy in each N$\hbar\omega$ space (to be more precise, the minimum of the expectation value of the SDPF.SM Hamiltonian plus the correction of equation 4, calculated for all the Slater Determinants of the m-scheme spherical basis). As we had anticipated the uncorrelated energies do not grow
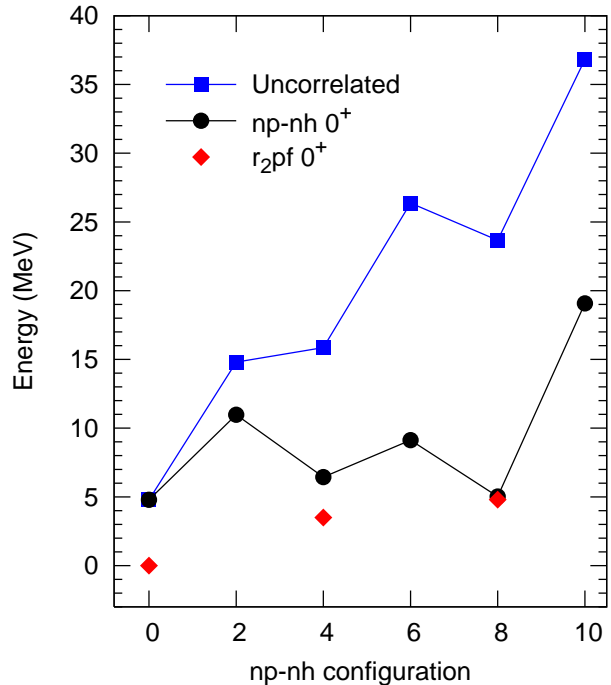

Figure 4: Energies in the different np-nh configurations; Lowest Slater Determinant plus the correction of equation 4 (squares); Energy of the lowest 0^+ state in the r_2pf space at fixed N$\hbar\omega$ (circles). The diamonds give the energies of the fully mixed calculations in the r_2pf space

linearly with the number of particles excited across the N=Z=20 gap (if it had been so, all the squares would lie in the prolongation of the straight line joining the n=0 and n=2 points). The increase is much slower, with a superimposed odd-even effect in n/2. Notice that energy of the lowest 8$\hbar\omega$ Slater Determinant lies $\approx$ 20 MeV above the closed shell. Finally, we carry out the explicit diagonalizations separately for each N$\hbar\omega$ value and we find the results plotted as circles. We can see that the correlation energies are very large, in particular for the SD bandhead that gains 18.5 MeV and becomes almost degenerated with the closed shell configuration. We can make a rough analysis of the correlation energies in terms of their T=0 and T=1 pairing and multipole-multipole (mainly quadrupole-quadrupole) content. For that we compute the expectation value of the (monopole free) pairing part of the effective interaction in the fixed n$\hbar\omega$ bandheads and subtract it from the total correlation energy. In the 4$\hbar\omega$ 0^+ ND state, out of the 9.5 MeV of correlation en-
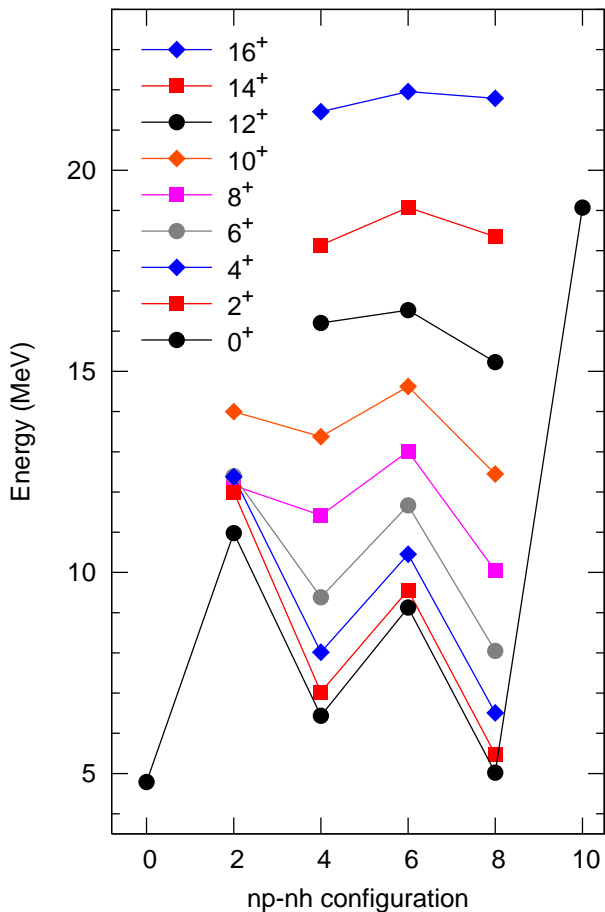
Figure 5: Energies of the yrast states in the fixed np-nh calculations (corresponding to the circles in Fig. 4 for J=0)

Table IV: Percentage of np-nh components and energy of the first three 0^+ states (GS, ND, and SD) of ^{40}Ca

	0p-0h	2p-2h	4p-4h	6p-6h	8p-8h	E(th)	E(exp)
0^+_{GS}	65	29	5	-	-	0	0
0^+_{ND}	1	1	64	25	9	3.49	3.35
0^+_{SD}	-	-	9	4	87	4.80	5.21

J=0^+ states, i. e. they are angular momentum projected solutions (before variation, VAP in the usual jargon). In Fig. 5 we add the points for all the lowest states of even J that appear in the deformed ($4\hbar\omega$ and $6\hbar\omega$) and superdeformed ($8\hbar\omega$) bands and the corresponding $2\hbar\omega$ and $10\hbar\omega$ states. We can observe that the structure of wells and barriers of the J=0 curve, that protects the deformed and superdeformed bands from strong mixing, is maintained up to J=10. Above, the barriers flatten and we should expect larger mixing. In particular this can lead to the erosion of the collectivity of the SD band at high spin in the calculation.

VI. RESULTS OF THE COMPLETE CALCULATIONS IN THE r_2pf SPACE

The calculations in the r_2pf space are computationally very demanding. In addition to the very large dimensions involved, the need to compute several states of the same angular momentum increases substantially the number of Lanczos iterations needed to achieve convergence. The shell model code ANTOINE [24] has been used throughout.

The structure of the first three 0^+ states, the spherical ground state and the excited deformed and superdeformed band-heads is shown in table IV. The two body cross-shell off diagonal matrix elements can connect directly configurations differing only in two particle hole jumps. We see in the table that, indeed, the ground state 0p-0h leading component is mainly correlated by 2p-2h components. The leading 4p-4h component of the ND state can, in principle mix with 2p-2h and 6p-6h components. Actually the mixing is dominated by the latter, with a non-negligible 8p-8h piece. The leading 8p-8h component of the SD could also mix with 6p-6h and 10p-10h configurations directly, but it chooses none. The SD band-head is very pure, with only small amounts of 4p-4h and 6p-6h components. Let us mention that the yrast band in the $6\hbar\omega$ space, corresponds also to a rotor with deformation slightly larger than the one in the $4\hbar\omega$ space. On the contrary, the deformation and the correlation energy in the $10\hbar\omega$ space are smaller, leading to negligible mixing with the other spaces.

In the process of mixing the winner is, energy wise, the ground state that gains almost 5 MeV, mostly pairing-like. The ND band gains barely 2 MeV and the SD band essentially nothing. That's why, in order to reproduce the

ergy, 5.5 MeV come from T=1 pairing, 0.5 MeV from T=0 pairing and 3.5 MeV from the quadrupole correlations. In the $8\hbar\omega$ 0^+ SD state, the share is 5.5 MeV, 0.5 MeV and 12.5 MeV respectively. Thus, the contribution of the neutron proton pairing amounts to 2.33 MeV for any of the bands.

The structure of the line joining the black circles in the plot in quite interesting, because it resembles the energy versus deformation curves typical of projected Hartree-Fock calculations. The number of particle-hole excitations in the X-axis can be taken as roughly proportional to the deformation. With this perspective, we distinguish three coexisting minima, spherical, n=0, deformed, n=4, and superdeformed, n=8, separated by the n=2 and n=6 maxima. The n=10 band-head lies very high in energy and we have verified that it plays no role at all in this problem. The structure of this "potential energy" curve, consisting of wells and barriers, provides an intuitive picture of how the deformed and superdeformed bands can preserve their identity after mixing.

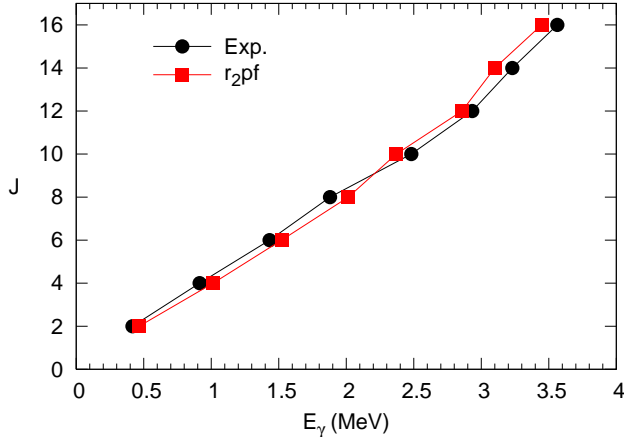Keeping on with the mean field analogy, it is worth to note that the black circles in Fig. 4 correspond to

Figure 6: E_γ's in the SD band, mixed calculation *vs.* experiment

experimental situation, the three 0^+ states before mixing must be degenerated or even with their energies inverted The energies of the three physical 0^+ states after mixing are represented by the diamonds in Fig. 4.

A. The Super-Deformed Band

We start the discussion of the results with the excitation energies of the SD band as produced by the fully mixed calculation. As we can see in Fig.6, the mixing does not modify noticeably the features already present in the fixed 8p-8h calculation. Perhaps one could detect some irregularities at the upper part of the band. The calculated sequence crosses the experimental one at around the rotational frequency where the calculated states start loosing collectivity, but in global terms, the agreement is excellent. The results of the mixed calculation beyond J=16 are equivalent to that of the fixed $8\hbar\omega$ calculation shown in Fig. 1

In table V, we give the np-nh structure of the SD band up to J=16. The 8p-8h component is nicely constant up to J=10, as we expected from the analysis of the potential energy curves in Fig.5. At higher angular momentum, the mixing with $6\hbar\omega$ components becomes stronger, and we should expect a less collective behavior. It is interesting to follow the evolution of the location of the SD states with increasing angular momentum. The J=0 SD state is the third J=0 state in the spectrum. The J=2, 4, and 6 states are the second of their spins, J=8 and 10, third, J=12, fourth, J=14 sixth, and finally J=16 fourth again.

We shall examine now the quadrupole properties of the superdeformed band in ^{40}Ca as they come out of the full r_2pf calculation. In table VI we have gathered the theoretical spectroscopic quadrupole moments and the B(E2) values. We can conclude that the mixing causes just an erosion of the $8\hbar\omega$ values presented in table I up

Table V: np-nh structure of the superdeformed band of ^{40}Ca.

J	0p-0h	2p-2h	4p-4h	6p-6h	8p-8h
0	-	-	9	4	87
2	-	-	11	4	85
4	-	-	8	5	87
6	-	-	3	5	91
8	-	-	2	6	91
10	-	-	1	12	87
12	-	-	2	29	69
14	-	-	11	27	63
16	-	-	0	40	60

Table VI: Quadrupole properties (in efm^2 and e^{2}fm^4) of the superdeformed band in ^{40}Ca. Full r_2pf calculation.

J	$Q_{spec.}$	B(E2)$_{J \to J-2}$	Q_0(s)	Q_0(t)
2	-47.7	579	167	171
4	-61.1	813	168	169
6	-66.3	874	166	167
8	-66.5	906	158	166
10	-66.3	844	153	158
12	-71.8	546	162	126
14	-62.1	557	139	127
16	-64.9	429	142	111

to J=10-12. Beyond, the larger presence of less collective $6\hbar\omega$ components has a much stronger effect, particularly in the B(E2)'s. Thus, the values of the transition quadrupole moments diminish rapidly at the end of the band. The static quadrupole moments vary less abruptly.

In Fig. 7 we compare our calculated numbers with the experimental results. Comparing with the fixed $8\hbar\omega$ results, we find a large reduction of the transition quadrupole moments of the three upper transitions of the band. It is possible that this drop in collectivity be an artifact of the r_2pf space, but for the moment we have no way to verify it.

The experimental points in the figure for J≥6 are those of the first analysis of the Doppler Shift Attenuation data made in ref.[10]. The J=4 point comes from another, earlier, experiment [26]. The calculated transition quadrupole moments agree with the data for J≤10, but underestimate them for the three uppermost transitions. In ref.[25] a reanalysis of the same experimental data was made, and the preferred solution differs from the precedent one. Whereas the former solution was a constant $Q_0(t) = 180^{+0.39}_{-0.29}$ e fm^2 for the six transitions from the states of the SD band with J=16 to J=6, the latter gives $Q_0(t) = 181^{+0.41}_{-0.26} \pm 0.21$ e fm^2 for the J=16 to J=12 states and $Q_0(t) = 118^{+0.06}_{-0.05} \pm 0.13$ e fm^2 for J=10 to J=6. Notice that, compared to ref.[10] an extra systematic error has been added. In spite of that, the final error bars of
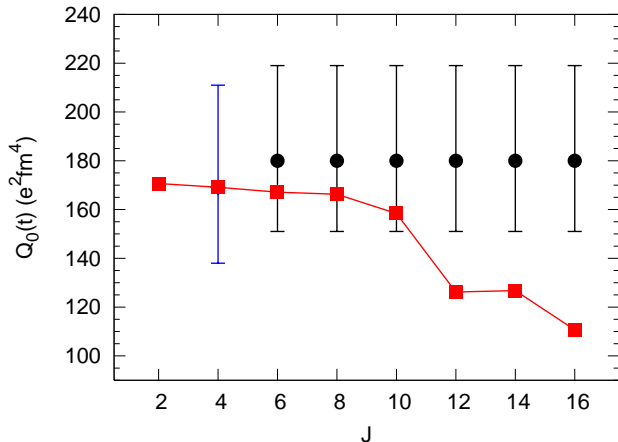
Figure 7: Transition quadrupole moments in the SD band. Full r_2pf results (squares) compared to the experimental data from refs. [26] (lozenges) and [10] (circles)

Table VII: np-nh structure of the deformed band of ^{40}Ca based on the first excited 0^+ state

J	0p-0h	2p-2h	4p-4h	6p-6h	8p-8h
0	1	1	64	25	9
2	-	1	64	24	10
4	-	1	68	23	8
6	-	2	75	20	3
8	-	21	62	15	2
10	-	-	81	17	1
12	-	-	81	18	1
14	-	-	82	17	1
16	-	-	79	19	1

the values corresponding to the lower J transitions are largely reduced with respect to those of the upper transitions. Actually, their extracted $Q_0(t)$ values are barely compatible with the value for the $4^+ \rightarrow 2^+$ 914 keV transition, $Q_0(t) = 169^{+0.42}_{-0.32}$ e fm^2, obtained in ref. [26] (the lower and upper tips of one and another error bars just touch at the value 137 e fm^2).

If the results of the analysis of Chiara *et. al.* were the only viable interpretation of the data, the comparison with our calculated $Q_0(t)$'s. would be rather poor, meaning that something important in missing in our approach. The beautiful agreement we had for J≤10 will be lost, and the fact that the increase of the experimental error bars for the upper transitions make our results deviate less, is a meager compensation. We have tested solutions with larger mixing, through the mechanisms discussed in section V, but even going as far as keeping just 50% of closed shell in the ground state, we obtain only an extra 10% erosion of the B(E2)'s for J≤10. On the contrary, more mixing brings in large reductions of the transitions in the upper part of the SD band. In the section dealing with the out-band decay branches we propose a mechanism that conciliates the theoretical picture with the experimental data. It is based on a detailed analysis of the decay of the J=8 member of the SD band, a decay that in our opinion, has driven the fit of ref.[25] into the new set of $Q_0(t)$'s.

B. The Normal-Deformed Triaxial Bands

We move now to the full r_2pf space results for the two bands that according to our calculations have a dominant 4p-4h structure. As we have shown in section IV they are consistent with the presence of a deformed triaxial intrinsic state. In table VII we list the percentage of the different np-nh components in the deformed band of ^{40}Ca based on the first excited 0^+ state. We observe that the 4p-4h dominance is less strong than the 8p-8h dominance in the SD band at low spins, and larger at high spins. Another characteristic feature is that the mixing proceeds through the 6p-6h components, with the 2p-2h components completely absent except in the J=8 state, where an accidental degeneracy occurs. We do not have a definite explanation for this preference, that can be due to phase space considerations (there are much more 6p-6h states to mix with than 2p-2h states) but more probably to the fact that the collectivity of the 4p-4h and 6p-6h spaces is very similar and much larger than that of the 2p-2h space. That the mixing strength of the 6p-6h space is exhausted by the ND band could explain why the SD band is so pure. As expected in a collective picture, the spread of the wave functions of the states of the γ band among the np-nh spaces is very similar to that of the ND band.

In Fig. 8 we plot the calculated energies of the ND band compared with the experiment. We observe that the mixing improves clearly the agreement in the lower part of the band. The discrepancy at the backbending is the same already present in the $4\hbar\omega$ calculation.

The 2^+ band-head of the γ band is predicted at 5.88 MeV of excitation energy compared with the experimental value 5.25 MeV. This means that the mixing increases the splitting of the ND and γ bands by 350 keV with respect to the result of the $4\hbar\omega$ calculation. The in-band excitation energies change very little with respect to the $4\hbar\omega$ values gathered in table II.

The quadrupole properties of the ND band –table VIII– are very similar to those of the $4\hbar\omega$ calculation. Only at J=8 there is a reduction in collectivity due to the accidental mixing with a nearby 2p-2h state that we have already commented. As can be seen in Fig. 9, where we have plotted the transition quadrupole moments, this reduction goes in the direction demanded by the data. Globally the agreement is quite good, the trends are very well reproduced and in most cases the theoretical numbers fall inside the experimental error bars. At the upper part of the band the theoretical values underestimate the
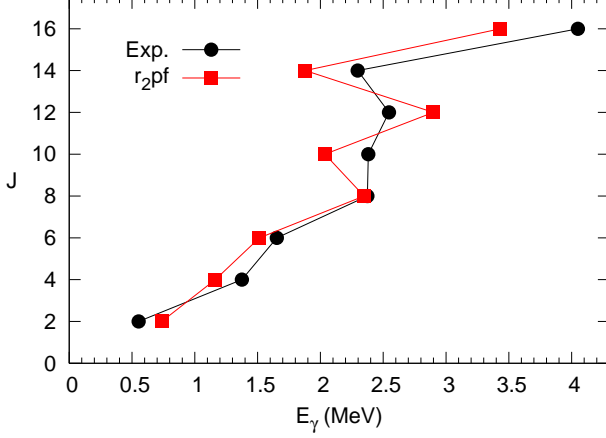
Figure 8: Deformed band in ^{40}Ca. E_γ's, experiment *vs* full r_2pf calculation.
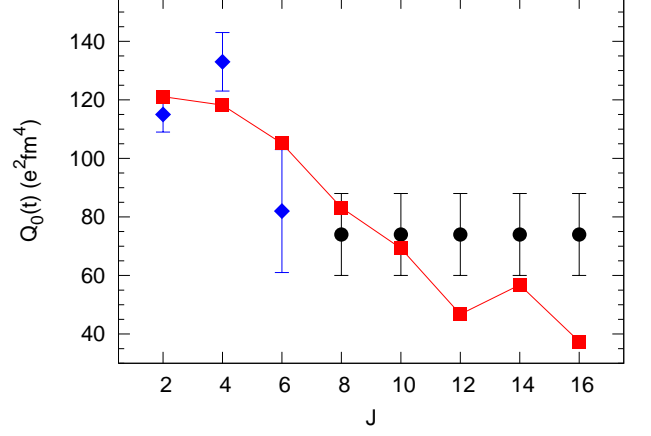

Figure 9: Transition quadrupole moments in the SD band. Full r_2pf results (squares) compared to the experimental data from refs. [27] (lozenges) and [10] (circles)

Table VIII: Quadrupole properties (in efm^2 and e^{2}fm^4) of the ND ^{40}Ca, r_2pf calculation

J	$Q_{spec.}$	B(E2)$_{J \to J-2}$	Q_0(s)	Q_0(t)
2	-32.2	292	113	121
4	-42.1	397	116	118
6	-47.3	346	118	105
8	-35.5	227	84	83
10	-48.1	161	111	69
12	-37.6	75	85	47
14	-39.1	112	87	57
16	-35.6	49	78	37

Table IX: Quadrupole properties (in efm^2 and e^{2}fm^4) of the γ band in ^{40}Ca, r_2pf calculation.

J	$Q_{spec.}$	B(E2)$_{J \to J-2}$	B(E2)$_{J \to J-1}$	Q_0(s)	Q_0(t)
2	28.6			100	
3	-0.24		427	-	
4	-17.7	133	284	122	106
5	-25.7	214		111	106
7	-33.5	211		104	90
9	-35.6	175		96	77
11	-45.9	110		115	59
13	-40.5	80		97	49

experimental ones. The data come from different sources, for the J≥8 they are taken from the Doppler Shift Attenuation analysis of ref. [10], for J=6 and J=8 from the lifetimes and branching ratios measured in refs.[26, 27].

In table IX we have collected the calculated quadrupole properties of the γ band. The intrinsic information has been extracted from the B(E2)'s and spectroscopic quadrupole moments assuming K=2. We find again a well defined deformed intrinsic state, with similar static and transition quadrupole moments, both very similar to those of the ND band.

C. Out-band transitions

The experimental data on out-band transitions are scarce and very often affected of large uncertainties. For the low energy part of the spectrum of ^{40}Ca lifetimes and branching ratios are known for some levels. These will be compared with our predictions in tables X and XII. For J≥6, we rely in the semi-quantitative informations of refs. [10] and [25]. In table X, we focus in the out-band

transitions from ND and SD states. The balance is uneven. The transition probabilities of the decays from the 2^+ states in the ND and SD bands to the ground state are largely under-predicted by the calculation. When we increase the mixing they increase at most by a factor two, very far from what would square with the data. For these small B(E2)'s it is possibly not sensible to reason in terms of factors, but instead think that some additive contribution is lacking in our space. It is worth to recall here that the span of B(E2) values that we are trying to explain simultaneously is of three orders of magnitude. The decay of the superdeformed 0^+ is well reproduced, and the same applies to the decay of the superdeformed 4^+ to the deformed 2^+. The in-band transition is simultaneously well accounted for (see Fig. 7), but apparently we miss badly the two remaining transitions known experimentally. We cannot but recognize our limitations.

In table XI we present the calculated B(E2)'s, E_γ's and the in-band branching ratios. For the experimental information we draw from the article by Chiara *et. al.* [25]. The calculated branching ratios for the three up-

Table X: Out-band transitions from the superdeformed (SD) and normal deformed (ND) bands of ^{40}Ca. The energies are in keV and the B(E2)s in e^2fm^4.

Transition		E_γ		B(E2)	
		Theory	Experiment	Theory	Experiment
$2^+_{ND} \to$	0^+_{GS}	4232	3904	1.8	18±1
$0^+_{SD} \to$	2^+_{ND}	565	1307	58	134.8±24.5
$2^+_{SD} \to$	0^+_{GS}	5263	5629	0.1	1.7±0.4
	0^+_{ND}	1769	2277	3	20.9±5.0
$4^+_{SD} \to$	2^+_{ND}	2045	2638	19.4	21±4
	4^+_{ND}	882	1264	6.8	116±34
	2^+_3	397	1294	2.7	176±41

Table XI: Comparison between the theoretical in-band ($SD \to SD$) and out-band transition probabilities ($SD \to ND$) for the states of the superdeformed band of ^{40}Ca with J≥6. The energies are in keV and the B(E2)s in e^2fm^4.

Transition		$B(E2)_{J \to J-2}$	E_γ	E_γ(th)	BR %
$6^+_{SD} \to$	4^+_{SD}	874	1432	1521	
	4^+_{ND}	43	2695	2403	46
$8^+_{SD} \to$	6^+_{SD}	906	1880	2015	
	6^+_{ND}	7.8	2921	2904	93
$10^+_{SD} \to$	8^+_{SD}	844	2481	2371	
	8^+_{ND}	12	3030	2929	96
$12^+_{SD} \to$	10^+_{SD}	546	2932	2857	
	10^+_{ND}	1.5	3.590	3750	100
$14^+_{SD} \to$	12^+_{SD}	557	3230	3100	
	12^+_{ND}	5.0	4264	3952	97
$16^+_{SD} \to$	14^+_{SD}	429	3563	3447	
	14^+_{ND}	0.03	5531	5520	100

permost transitions of the SD band are close to 100% in agreement with the experimental observation. For the next transition, the predicted 96% branching ratio looks too large when inspecting the figure in ref. [25], but the paper does not give a figure for it. However, it is in the decay of the 8^+ member of the superdeformed bands that we depart dramatically from the experimental branching ratio, 96% calculated *vs* 20% experimental. We shall devote some space to this comparison, mainly because it is in our opinion due to this very number that the authors of ref. [25] obtain a fit to their Doppler Shift Attenuation data in which, for J≤10, the transition quadrupole moments of the band have values that correspond actually to a normally deformed band. Before that, let's mention that the branching ratios of the 6^+ SD state seem also consistent with the data of Chiara *et al.* and with a rather pure superdeformed character. We have already seen that the calculation also describes correctly the 4^+ SD branching ratios.

Our argument goes as follows: Given that the phase space factors favor the out-band transition by a factor 9, and considering that the B(E2)'s of the $8^+_{SD} \to 6^+_{SD}$ and $8^+_{ND} \to 6^+_{ND}$ in tables I and III are 980 e^2fm^4 and 309 e^2fm^4 respectively, it is readily seen that the experimental branching ratio cannot be reproduced unless the 9307 keV and 9856 keV experimental states correspond to a 50% mixing of the pure SD and ND states. Assuming that the J=6 states are pure ND and SD, this leads to BR=27%, with in-band B(E2)= 490 e^2fm^4 and out-band B(E2)= 150 e^2fm^4. The in-band transition in the ND band should have also B(E2)= 150 e^2fm^4. If we further assume that the J=10, 12338 keV, state of the SD band is pure, it will decay equally to the 9307 keV and 9856 keV J=8 states, which seems to be the experimental situation. Translating this into transition quadrupole moments, we should have $Q_0(t)(10^+)$=118 e fm^2 and $Q_0(t)(8^+)$=122 e fm^2 in the super-deformed band and $Q_0(t)(8^+)$=69 e fm^2 in the normally deformed band, in excellent agreement with the experimental analysis of refs. [10, 25]. As a bonus, the low spin part of the band remains truly superdeformed. Actually the band is superdeformed all along except for the 8^+ state, even if the accidental degeneracy of the ND and SD 8^+ states provokes a strong reduction of the B(E2)'s of the transitions to and from the latter state. In addition, the lifetime of the 9856 keV, J=8, state is reduced by about a factor two.

Then, why are these features absent in our calculation? It is clear that in order to obtain a 50% mixing of the ND and SD states, they must be degenerate before mixing, their effective splitting being not larger than about 200 keV. To match this requirement is beyond the accuracy of our theoretical description. Paradoxically, the calculated excitation energies of the 9307 keV and 9856 keV J=8 states, 9260 keV and 9820 keV look astonishingly precise. But we fail to have the first excited 8^+ state, experimentally at 8103 keV at the right energy; it its predicted at 8900 keV. This state has a 2p-2h aligned nature and the fact that it mixes strongly with the ND state, that we have already discussed, means that both are degenerate before mixing at about their mean excitation energy.

In a sense, the character of the SD band is closer to what is suggested by the calculated static quadrupole moments in table VI. The only modification brought in by the 8^+ anomaly would be a reduction of its $Q_0(s)$ from 165 e fm^2 to 135 e fm^2

Finally, in table XII we have collected the out band transitions of the low spin states of the ND γ band. The experimental information is taken from ref. [27]. Our first concern is to figure out to which extent our hypothesis of low K-mixing is correct in the calculation. For that we compare the $2^+_\gamma \to 0^+_{ND}$ and the $2^+_{ND} \to 0^+_{ND}$ B(E2)'s, the former being twenty times smaller. A similar reduction is found in the $4^+_\gamma \to 2^+_{ND}$ *vs* $4^+_{ND} \to 2^+_{ND}$ case, thus confirming the validity of our assumption. The γ energies compare quite well with the experimental re-

Table XII: Out-band transitions from the γ band of ^{40}Ca. The energies are in keV and the B(E2)s in e^2fm^4.

Transition	B(E2)		E_γ	
	Theory	Experiment	Theory	Experiment
$2_\gamma^+ \rightarrow 0_{GS}^+$	0.20	1.0±0.3	5690	5249
0_{ND}^+	16	100±3	2277	1896
2_{ND}^+	91	179±50	1575	1343
$3_\gamma^+ \rightarrow 2_{ND}^+$	28	27±5	2295	2125
$4_\gamma^+ \rightarrow 2_{ND}^+$	20	32±7	2738	2603
4_{ND}^+	49	49±34	1632	1229

sults. The B(E2)'s are in excellent agreement with the experiment in all but one case, the corresponding to the $2_\gamma^+ \rightarrow 0_{ND}^+$ transition that is severely under-predicted. Even so, the experimental value is three time smaller than the equivalent transition inside the ND band.

D. Other approaches

There has been two other recent attempts to explain theoretically the structure of ^{40}Ca such as we know it after the experimental findings of Ideguchi *et al.* [10] and Chiara *et al.* [25]. Bender *et al.* [12] approach the problem in the framework of the constrained Hartree-Fock-BCS approximation. This is a calculation in the intrinsic frame, that is perfected by means of angular momentum and particle number projections. In a further step, the angular momentum projected solutions corresponding to different values of the deformation are mixed using the Generator Coordinate Method. Modern Skyrme parametrizations are used as effective interactions. They produce a ND and a SD band with a span much larger than the experimental one. The calculations are carried out only up to J=6 for the ND and J=10 for the SD band. They assume an axially symmetric basis, therefore precluding the description of the experimental γ band. Their ground state has a structure very similar to ours. For the SD band their predicted transition quadrupole moments are quite large, but the agreement with the data is incomplete. No calculation of out-band transitions is reported. There is a discussion of the np-nh structure of the states that we find difficult to translate into our language. They claim that the ND and SD bands do not have a well defined np-nh structure contrary to what our results show. However, our percentages of np-nh components cannot be compared with theirs directly. The second one applies the techniques of Antisymmetrized Molecular Dynamics [16]. They use an schematic interaction of Gaussian type. The calculation produces many excited bands, and, in particular, the three bands that we have studied in this paper. As we do, they obtain a superdeformed band of 8p-8h na-

ture. Their energetics is not very satisfactory. The ND band-head, that is experimentally the first excited state, is calculated about 5 MeV too high, while the lowest 0^+ pertains to an oblate side band not present in the experimental data. A bunch of states of unknown nature (J=2, 4, 6, and 8) are even lower. The SD band is also high but lower than the ND band. The splittings in the SD band look healthy, but the ND band does not resembles at all to a band. The γ band appears also at very high energy. Concerning the transition probabilities they are reasonable for the ND band and rather small for the SD band. No out-band transitions are reported.

VII. CONCLUSIONS

In this article, we have shown that large scale shell model calculations in a valence space comprising two major oscillator shells, can describe the coexistence of a doubly magic ground state and deformed and superdeformed bands in ^{40}Ca. We have explored the role of the spherical mean field and the correlations in bringing the n-particle n-hole configurations at very low excitation energy. We have examined the mechanisms of mixing between different np-nh configurations, and have analyzed the structure of the physical states in terms of these configurations. We find that the normally deformed bands are dominated by 4p-4h configurations with important mixing of 6p-6h components. The superdeformed band is clearly dominated by the 8p-8h configurations with small 6p-6h and 4p-4h contributions. We submit that for J=8 the ND and SD bands are accidentally degenerated and mix at 50%. The ND intrinsic structure is triaxial and produces a γ band. In the ground state, the doubly magic configuration amounts to 65%, mixed mainly with 2p-2h states. The comparison of the theoretical predictions with the experimental data for the energetics of the three above mentioned bands is excellent. We have computed also the electromagnetic transition probabilities for inband and out-band transitions. With some exceptions, the agreement is also very good. In addition to the challenge of accounting for super-deformation in a spherical shell model basis, *i. e.* in the laboratory frame, our calculations and modeling support the experimental claims on the existence of superdeformed bands at low excitation energy in this mass region, even in doubly magic ^{40}Ca.

[1] E. B. Carter, G. E. Mitchell and R. H. Davis, Phys. Rev. **133**, 1421 (1964).

[2] P. Chevallier, F. Scheibling, G. Goldring, I. Plesser and M. W. Sachs, Phys. Rev. **160**, 827 (1967).

[3] G. E. Brown and A. M. Green, Nucl. Phys. **A75**, 401 (1966).

[4] W. J. Gerace and A. M. Green, Nucl. Phys. **A93**, 110 (1967).

[5] W. J. Gerace and A. M. Green, Nucl. Phys. **A123**, 241 (1969).

[6] A. P. Zuker, B. Buck and J. B. McGrory, Phys. Rev. Lett. **21**, 39 (1968).

[7] R. Middletown, J. D. Garrett and H. T. Fortune, Phys. Lett. **B39**, 339 (1972)

[8] D. Rudolph, *et al.*, Phys. Rev. Lett. **82**, 3763 (1999).

[9] C. E. Svensson, *et al.*, Phys. Rev. Lett. **85**, 2693 (2000).

[10] E. Ideguchi, *et al.*, Phys. Rev. Lett. **87**, 222501 (2001).

[11] D. C. Zheng, L. Zamick and D. Berdichevsky, Phys. Rev. C **38**, 437 (1988).

[12] M. Bender, H. Flocard and P.-H. Heenen, Phys. Rev. C **68**, 044321 (2003).

[13] R. R. Rodríguez-Guzmán, J. L. Egido and L. M. Robledo, Intl. J. of Mod. Phys. **E**13, 139 (2004).

[14] G.-L. Long and Y. Sun, Phys. Rev. C **63**, 021305 (2001).

[15] T. Sakuda and S. Ohkubo, Nucl. Phys. **A744**, 77 (2004).

[16] Y. Kanada-En'yo and M. Kimura, Phys. Rev. C **72**, 064322 (2005)

[17] E. Caurier, F. Nowacki, and A. Poves, Phys. Rev. Lett. **95**, 042502 (2005).

[18] A. Poves, E. Caurier, F. Nowacki and A. Zuker, Eur. Phys, J. A **20**, 119 (2004).

[19] E. Caurier, F. Nowacki, A. Poves and A. Zuker, arXiv nucl-th/0205036.

[20] D. J. Rowe, G. Thiamova and J. L. Wood, Phys. Rev. Lett. **97**, 202501 (2006).

[21] A. Arima, M. Harvey, and K. Shimizu, Phys. Lett. **B30**, 517 (1969), K. Hecht and A. Adler, Nucl. Phys. **A137**, 129 (1969).

[22] A. P. Zuker, *et al.*, Phys. Rev. C **52**, R1741 (1995).

[23] A. P. Zuker, in *Contemporary Nuclear Shell Models*, X.-W. Pan, D. H. Feng, and M. Vallieres, eds. Lecture Notes in Physics (Springer, 1997) p.93.

[24] E. Caurier, *et al.*, Rev. Mod. Phys. **77**, 427 (2005).

[25] C. J. Chiara, *et al.*, Phys. Rev. C **67**, 41303 (2003).

[26] J. L. Wood, *et al.*, Phys. Rep. **215**, 101 (1992)

[27] P. M. Endt, Nucl. Phys. **A521**, 1 (1990).